metals

MDPI

Article

Study of Trivalent Chromium Conversion Coating Formation at Solution—Metal Interface

Wentao Sun [1], Guixue Bian [2], Luanluan Jia [3], Junjun Pai [3], Zonghao Ye [4], Ning Wang [1], Jiantao Qi [1,*] and Tengjiao Li [5,*]

[1] College of New Energy, China University of Petroleum (East China), Qingdao 266580, China
[2] Department of Aeromechanical Engineering, Qingdao Branch Naval Aviation University, Qingdao 266041, China
[3] Shandong Key Laboratory of Advanced Aluminum Materials and Technology, Binzhou Institute of Technology, Binzhou 256200, China
[4] Institute of Process Equipment, College of Energy Engineering, Zhejiang University, Hangzhou 310027, China
[5] The Boiler & Pressure Vessel Safety Inspection Institute of Henan Province, Zhengzhou 450000, China
* Correspondence: jiantao.qi@upc.edu.cn (J.Q.); ltj523@126.com (T.L.)

Abstract: The present study employed a tungsten pH microelectrode to study the formation of trivalent chromium conversion (TCC) coatings on Al, AA 2024-T3 aluminum alloy and AZ91D magnesium alloy in SurTec ChromitAL solutions. The tungsten microelectrode had a sensitivity of –60 mV/pH in the SurTec ChromitAL solutions. The peak and final pH values for pre-treated Al, AA 2024 alloy and AZ91D alloy were 4.9 and 3.5, 4.3 and 4.1, 4.7 and 3.5, respectively. The initial pH value is of great importance in influencing coating deposition-driven force and final coating thickness. In addition, the time to attain the peak values was 10, 100 and 20 s for Al, AA 2024 alloy and AZ91D alloy, respectively. The interfacial pH evolution is associated with the hydrolysis process of the weak acid nature of zirconium and chromium salts as the main components of TCC coating solutions. Raman spectra revealed the presence of chromium and zirconium oxides and sulphate in the solution deposits from in-house Cr/Zr and SurTec ChromitAL solutions.

Keywords: trivalent chromium; conversion coating; interface; tungsten microelectrode; pH; magnesium; aluminum

check for updates

Citation: Sun, W.; Bian, G.; Jia, L.; Pai, J.; Ye, Z.; Wang, N.; Qi, J.; Li, T. Study of Trivalent Chromium Conversion Coating Formation at Solution—Metal Interface. *Metals* **2023**, *13*, 93. https://doi.org/10.3390/met13010093

Academic Editor: Elena Gordo

Received: 7 December 2022
Revised: 24 December 2022
Accepted: 28 December 2022
Published: 1 January 2023

Copyright: © 2023 by the authors. Licensee MDPI, Basel, Switzerland. This article is an open access article distributed under the terms and conditions of the Creative Commons Attribution (CC BY) license (https://creativecommons.org/licenses/by/4.0/).

1. Introduction

Chromate conversion coating can be considered as one of the methods for the protection of light metals and alloys [1–8]. In consideration of the toxic and carcinogenic threat to human beings, chromate-related processes have been highly restricted [9–13]. In this sense, trivalent chromium conversion coating is a promising alternative and acceptable to meet industry requirements [14]. The formation mechanism of TCC coating is that it reacts at the solution–metal interface driven by pH to produce Cr/Zr hydroxide deposits, which are the main components of the coating [15–20].

TCC coating solution contains trivalent chromium sulfate, sodium hexafluoroalkanoate, sodium fluoride and other additives, and the recommended pH value for film formation is 3.8–4.0, and the temperature is 40 °C [21]. The coating formed was 50–100 nm thick. Qi et al. employed TEM to reveal the coating-formation kinetics of AA2024 alloys as a linear function of 0.23~0.27 nm/s (0~120 s) and 0.04~0.05 nm/s (>120 s) [22]. Corrosion resistance in 0.05 M NaCl solution was reported to be in the range of 10^5–10^6 Ohm cm^2 [23,24]. Notably, the post-treatment using a H_2O_2-conatining oxidant for 30 min significantly increased corrosion-protection performance to reach 4×10^6 Ohm cm^2, while the chromate species were only present at the surface with 0.1 wt.% coating components [25–28].

With respect to the localized corrosion of a tiny dimension, a cathodic reaction such as oxygen-reduction reaction (ORR) or hydrogen-evolution reaction (HER) results in a

pH increase nearby [29,30]. However, traditional pH glass electrodes fail in a minimal and localized corrosion area [16,31]. In addition, conversion-coating formation is a pH-driven process due to proton reduction, such as ORR and/or HER at the solution–metal interface [22]. In this sense, such chemistry information of proton-reduction reaction also requires local investigation using tiny microelectrodes.

Swain et al. developed a tungsten microelectrode to measure the in-situ pH change from 3.9 up to 4.4 close to the surface of AA2024-T3 alloy during immersion in hexafluorozirconate solution for 10 min [31,32]. The coating on the Al alloy was about half the thickness of that of aluminum, which was ≈ 100 nm on the latter [16]. Such coating differences was associated with the pH parameter. However, pH parameters for coating formation on aluminum, aluminuim alloys and magnesium alloys are little understood.

In the present study, a tungsten microelectrode was investigated using high-resolution optical and scanning electron microscopies. The comparison of interfacial pH evolutions during TCC-coating formation on aluminum and its alloys and magnesium alloys has been made with consideration of the aqueous chemistry. The coating -ormation mechanism based on the pH-driving force is further discussed.

2. Experimental Part

2.1. Sample and Microelectrode Materials and Their Preparation Procedures for TCC Formation

High purity aluminum (Shenyang Aircraft Industry Group, China) of 30 × 12 × 0.3 mm dimensions, was rinsed with acetone, ethanol and deionized water sequentially, and then a 20 V voltage was applied. The temperature was lower than 10 °C, lasting for 240 s, and aluminum was used as the counter electrode to electropolish the aluminum sample. The electropolishing solution consisted of a mixture of 20 vol% perchloric acid (60 weight%) and 80 vol% ethanol [16]. AA 2024-T351 alloy (Shenyang Aircraft Industry Group, Shenyang, China) with a composition the same as that reported in the previous report was etched in 5 wt.% NaOH for 60 s at 60 °C and de-oxidized in 50 vol.% HNO_3 for 30 s at ambient temperature, with a size of 30 × 20 × 3 mm. In addition, AZ91D magnesium alloy (Handan Fengfeng Longhai Metal Magnesium Processing Co., Ltd., Handan, China) with a composition of 9.12 wt.% Al, 0.68 wt.% Zn and 0.18 wt.% Mn was mechanically ground to a 5000 grit SiC finish and finely polished with 1.0 μm diamond paste. The size of the magnesium alloy was 30 × 20 × 5 mm. The pre-treated aluminum and its alloys and magnesium alloy were cleaned with deionized water and dried in a stream of cool air. (All the chemical reagents used in the above experiments were produced by Sinopharm Chemical Realgent Co., Ltd., Shanghai, China)

SurTec 650 chromitAL (SurTec International Gmbh, Bensheim, Germany) was used as the trivalent chromium conversion coating solution at 40 ºC, diluted with deionized water at 1:4 v/v. In addition, the in-house Cr/Zr solutions consisted of 0.02 M K_2ZrF_6 and 0.02 M $KCr(SO_4)_2$. The pH values of TCC coating solutions were adjusted to 3.9 by addition of some 5 wt.% H_2SO_4 and/or 1 wt.% NaOH droplets.

The tungsten microelectrode was prepared by alkaline etching of pure tungsten wire (99.999% purity, 0.1 mm in diameter) in 3 M KOH at constant voltages of 12 V for 20 s. A platinum ring with a diameter of 3.5 mm was used for the cathode and the tungsten working electrode was immersed in alkaline solution near the center of the platinum ring. Hydrogen bubbles were generated on the tungsten wire during etching due to the reduction of water molecules at the tungsten surface, accompanied by tungsten dissolution at the air–solution interface, according to the reaction [33].

$$W(s) + 2OH^- + 2H_2O \rightarrow WO_4^{2-} + 3H_2(g) \quad (1)$$

After alkaline etching, the tip was ultrasonically cleaned in ultrapure water for 10 min and cooled with compressed air. Asphalt was used to cover the fresh tip, avoiding air oxidation. Before the interfacial study, the asphalt-covered tip was opened by employing evaporation combustion of the asphalt near a hot resistance wire [34].

2.2. Installation Scheme and Characterization of Electrolyte pH for TCC Formation, Equipment for Microanalysis and Raman Spectroscopy of Objects of Study and MEDUSA Software for Simulating Chemical Reactions

The open-circuit potential (OCP)—pH calibration of the tungsten microelectrode and measurements of pH changes during coating formation were made using a two-electrode system with a CorrTest CS 310 electrochemical workstation (Wuhan, China). A saturated calomel electrode (SCE, 0.24 V vs NHE) as the reference and counter electrode (RE/CE) was employed and the tungsten microelectrode was the working electrode (WE). For studies of coating formation, the specimen part was immersed in the solutions and the distance between the microelectrode and specimens was adjusted to 1–2 μm with the assistance of a high-resolution USB Digital Microscope (X300, MUSTECH, Shenzhen, China) and XYZ control system with a resolution of 1 μm. Figure 1a displays the schematic explanation of the pH investigation at the solution–metal interface employed two-electrode system, where the red arrow outlines the well-prepared tungsten-tip microelectrode. Figure 1b shows an image of the illustration set-up and SCE electrode with the reference and counter electrode (RE/CE) and tungsten microelectrode as the working electrode (WE). The set-up, shown schematically in Figure 1, was located on a shock absorbing platform.

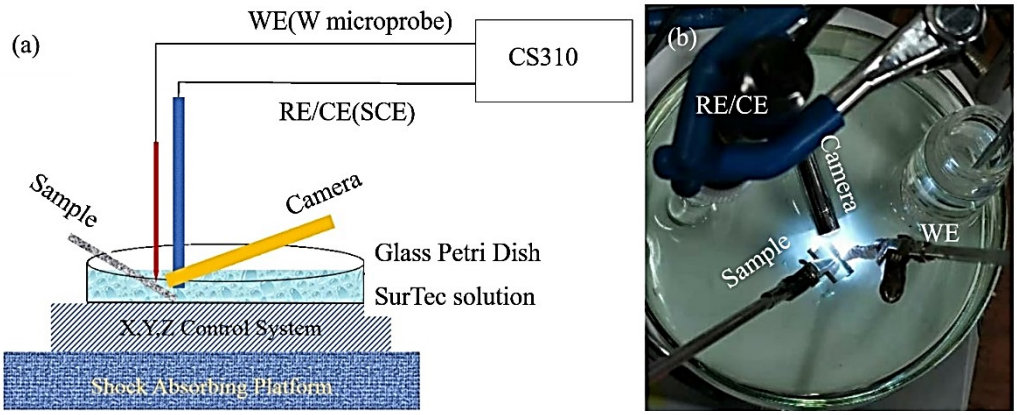


Figure 1. (**a**) Schematic explanation of the pH investigation at the solution–metal interface employed two-electrode system, where the red arrow outlins the well-prepared tungsten-tip microelectrode; (**b**) The image of the experimental set-up and SCE electrode with the reference and counter electrode (RE/CE) and tungsten microelectrode as the working electrode (WE).

Scanning electron microscopy (SEM) with energy-dispersive X-ray spectroscopy (EDS) (ZEISS Cross beam 550 instrument, Germany) was employed to examine the microelectrode, with an accelerating voltage of 15 kV. The pH values in the bulk solutions were measured using a pH meter (PSE-3E, INESA, China) with temperature compensation.

Horiba LabRAM HR Raman spectroscopy was used to observe the chemical composition of the SurTec conversion film. Raman spectra were recorded under a 532 nm laser source (CW), Olympus optical microscope (objective magnification 50×) and exposure time of 10–30 s without accumulation treatment.

In terms of the aqueous chemistry balance, the open-access software, MEDUSA (Version 3, developed by the Royal Institute of Technology (KTH), was used to calculate the complexes and phases in a given chemical solution using the equilibrium formation constants at room temperature and varied ionic strength (mol/(kg H_2O)) [35,36].

3. Results and Discussion

3.1. Tungsten Microelectrode and Calibration

Figure 2a,b shows high-resolution SEM images of a conically shaped, fresh tungsten microelectrode etched in 3 M KOH solution and the asphalt-covered tungsten microelectrode, respectively. The length and diameter of the unsealed tip were 100 and 1.5 μm, respectively. In contrast, the exposed length of the sealed tip was ~40 μm to increase the

investigation sensitivity at the solution–metal interface. The tip in Figure 1a was bent due to the sample moving to the SEM investigation stage. In addition, contaminations were observed in Figure 1b and they may have come from the environment.

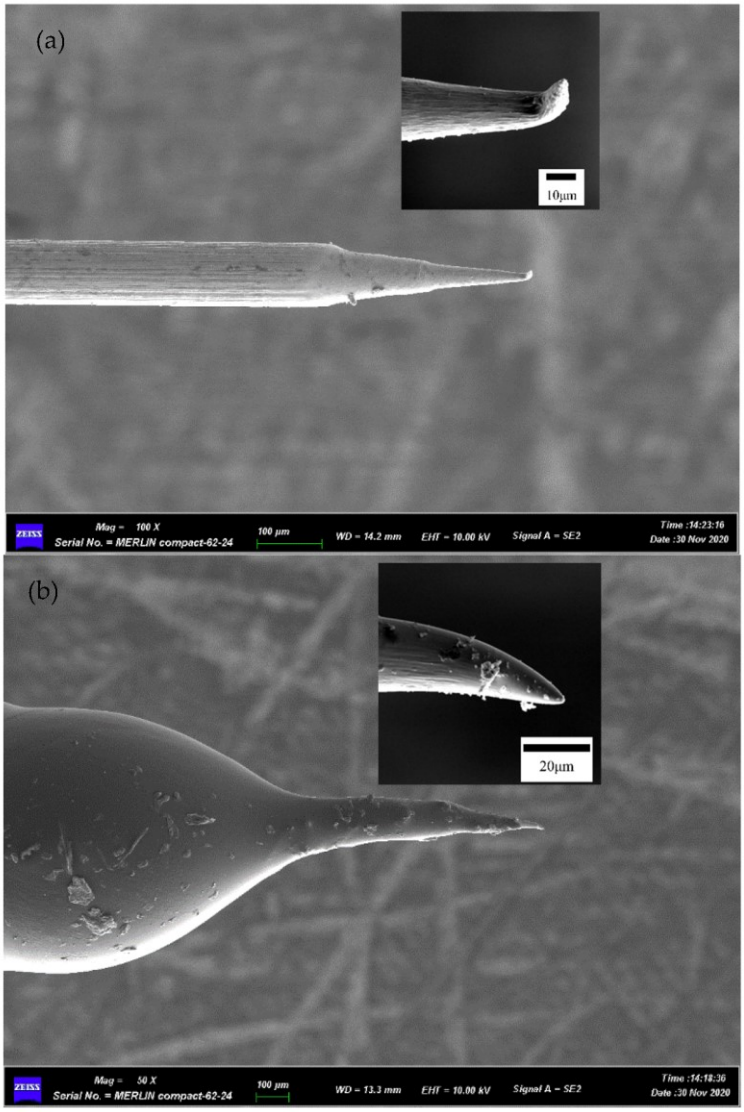


Figure 2. SEM images of the conically shaped tungsten microelectrode etched in 3 M KOH solution, including (**a**) the bare microelectrode and (**b**) the asphalt-covered microelectrode. The inserted images were with high magnification.

Figure 3 displays the calibration curve of potentials and pH of the deionized water with adding 5% H_2SO_4 versus 5% NaOH droplets containing buffers of pH at 2.1, 2.55, 3.07, 3.5, 4.11 and 4.66, revealing a linear relation of OCP (mV) = −65.32 Ph—44.8 and hence, a sensitivity of −65.32 mV/pH.

To determine the sensitivity of the tungsten microelectrode in the SurTec 650 ChromitAL solution, the tungsten microelectrode was used as the working electrode in a two-electrode system. The pH values of the SurTec solutions adjusted by 5% NaOH and/or 5% H_2SO_4 droplets were 2.48, 2.88, 3.32 and 3.77. Figure 4 shows a linear relationship of OCP (mV vs SCE) of −194.25—60 pH and hence, a sensitivity of −60 mV/pH. Swain et al. reported a sensitivity of –64 mV per pH in phosphate and hexafluorozirconate buffers [31]. In comparison, the aqueous chemistry balance at the tungsten tip in the present H2SO4 and SurTec buffers at 40 °C was comparable with that reported above. Notably, the OCPs investigated by the asphalt-covered microelectrode in Figures 3 and 4 were negative shifts

relative to that reported by Swain et al. For example, the OCPs by the asphalt-covered and Swain's microelectrode in the SurTec and hexafluorozirconate solutions of pH 3.8 were −422.2 and −14.4 mV, respectively. The reason is due to the difference of insulation materials for the fresh microelectrode and the exposed tip size. In comparison, the exposed size in the present study was reduced by three times that employed in the previous report. In addition, the polymer insulation may have played a negative resistance role in the acidic environment [31].

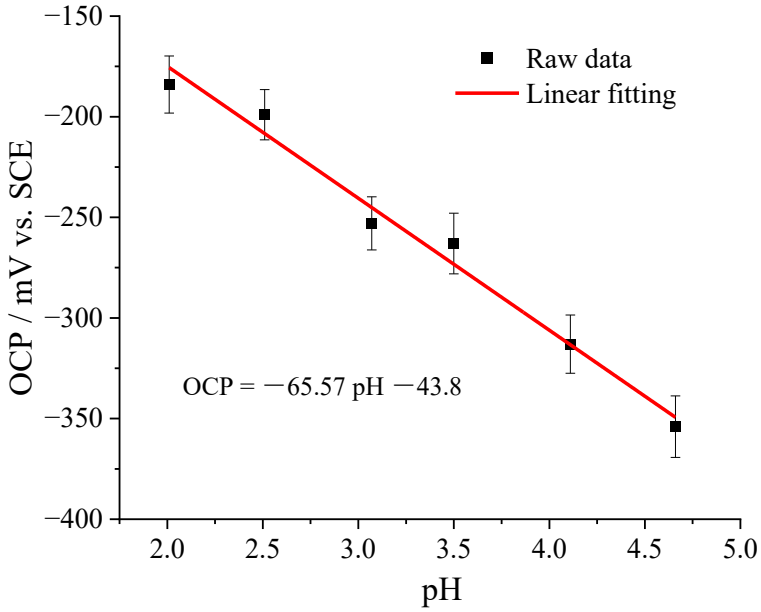


Figure 3. Plots of open circuit potentials and pH of the deionized water with adding 5% H_2SO_4 and 5% NaOH droplets as functioned as "OCP = −65.57 pH—43.8".

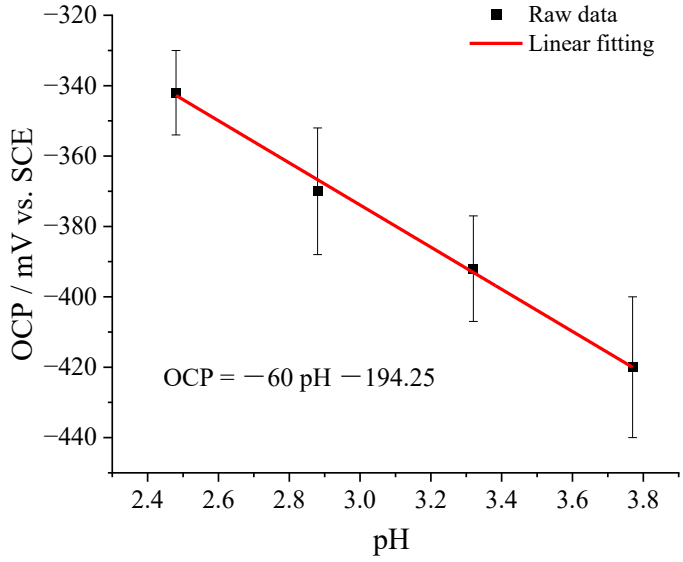


Figure 4. Plots of open circuit potentials and pH of SurTec 650 ChromitAL solutions with adding 5% H_2SO_4 and 5% NaOH droplets with raw and fitted data as functioned as "OCP = −60 pH—194.25".

3.2. Comparison of the pH Evolution at Light Alloys–Solution Interface

Figure 5 displays the plots of potentials versus pH with respect to time for (a) electropolished Al, (b) AA 2024 alloy after NaOH etching and HNO_3 de-oxidation and (c) finely polished AZ91D alloys in the SurTec 650 ChromitAL solutions (40 °C).

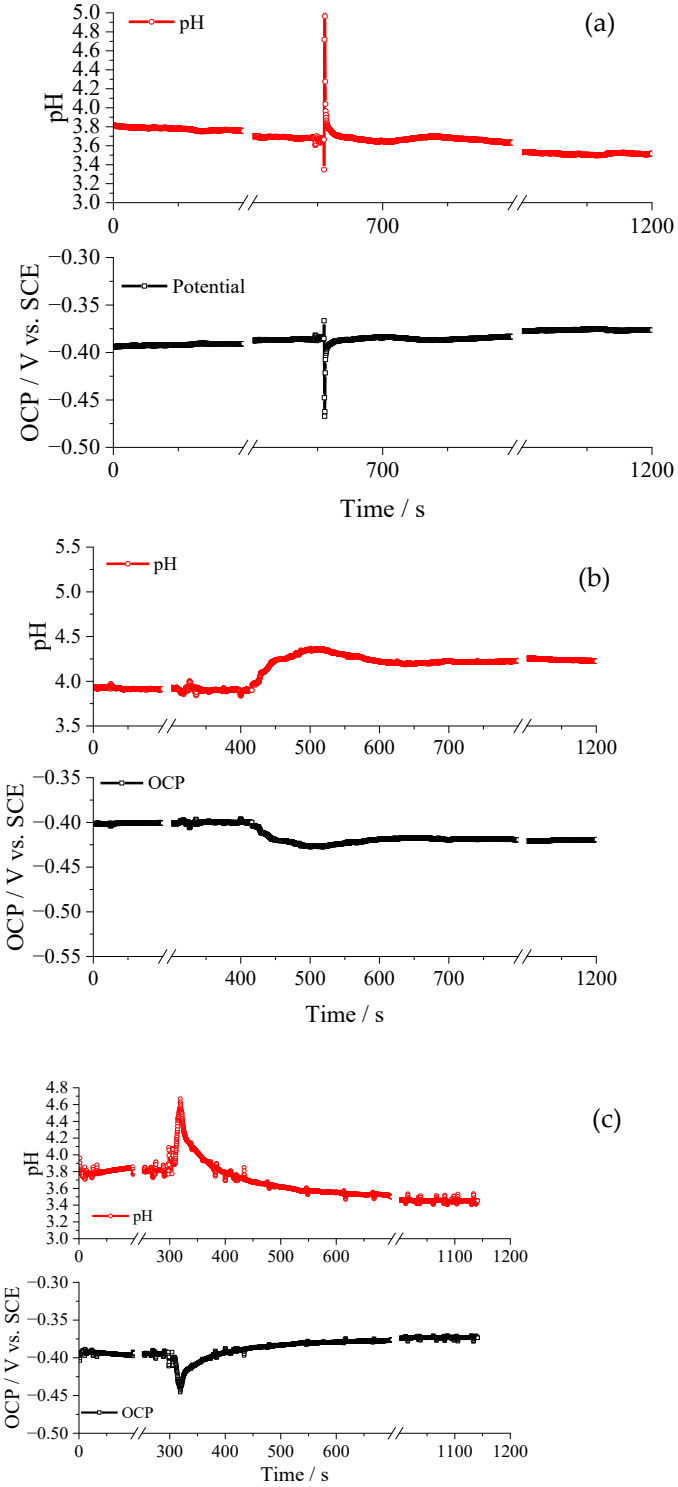


Figure 5. Plots of open circuit potentials and pH with respect to time for (**a**) electropolished Al, (**b**) AA 2024 alloy after NaOH etching and HNO_3 de-oxidation and (**c**) finely polished AZ91D alloys in the SurTec 650 ChromitAL solutions (40 °C).

Prior to immersion of the samples, the microelectrode registered a stable pH of 3.8–3.9, which is consistent with the findings in Figure 4. The specimen was then gently immersed, and the camera was focused on the microelectrode tip to assist in setting the distance between the tip and the aluminum surface to ≈1.5 µm (the tip diameter). The interfacial pH value was functioned with respect to the OCP evolution with a sensitivity of –60 mV/pH as measured in Figure 4.

The formation of trivalent chromium coating is a pH-driven process. The cathodic reaction (oxygen absorption or hydrogen evolution reaction) at the metal–solution interface consumes hydrogen ions (hydrogen radical ions are produced), and the pH rises, which causes metal ions in the solution to form the corresponding hydroxide deposit. Compared with Table 1 and Figure 5, the higher pH peak value, the faster the coating component deposition. Notably, the interfacial pH value was associated with the potential as suggested by the Pourbaix diagram based on thermodynamics [37]. In this sense, the higher pH value during coating formation on Al was indicative of lower surface potentials as found below.

Table 1. Thickness of trivalent chromium conversion coating on different materials.

Material	Thickness	Time	Reference
Aluminum	162 nm	1200 s	[38]
2024-T3	75 nm	1200 s	[31,39]
AZ91D	75 nm	1200 s	[22,25,40]

The time of sample immersion in the SurTec solution and close to the tungsten micro-electrode was 650, 425 and 300 s for the samples in Figure 5a–c, respectively. The mechanical operation for the sample immersion and movement induced a sudden vibration as observed in the OCP evolution plots. In comparison, the peak and final pH values for pre-treated Al, AA 2024 alloy and AZ 91D alloy were 4.9 and 3.5, 4.3 and 4.1, 4.7 and 3.5, respectively. In addition, the time to reach the peak value was 10, 100 and 20 s for the respective samples above. In comparison, the pre-treated AA 2024 alloy revealed the lowest peak and largest final pH values and this was possibly due to the homogenous surface after etching and de-oxidation pre-treatments. Notably, the final pH values for the pure aluminum and polished magnesium alloys were lower than that in the bulk solutions. The local acidity was associated with the continuous chemical attack by single fluoride ions while such ions were blocked by the intact coatings on the pre-treated aluminum alloys [16,22]. In this sense, the pH evolution variance between the electropolished Al and the pre-treated Al alloys gave rise to the coating-thickness difference after the conversion-treatment process. In addition, the initial pH value played the key role influencing the driven force of coating deposition [37].

3.3. Plots of Aqueous Chemistry Balance Simulated with MEDUSA Software

Figure 6 displays the simulated plots of the aqueous chemistry in the 0.024 M K_2ZrF_6 solution at room temperature. In the range of pH 4–6, the concentration of single fluoride ions increased and the limited pH values for zirconium oxide deposits were around 4.2.

Figure 7 displays the simulated plots of the aqueous chemistry in 0.01 M $Cr_2(SO_4)_3$ solution at room temperature. The limiting pH values for chromium hydroxide and oxide deposits were 3.2 and 3.6, respectively. Figure 8 displays the simulated plots of the aqueous chemistry in the 0.02 M $Cr(NO_3)_3$ solution at room temperature. The limiting pH values for chromium hydroxide and oxide deposits were 3.8 and 4.0, respectively. In comparison, the limiting pH values for chromium-containing deposits were influenced by the anion type. Wen et al. studied the influence of anions of chromium salts on the microstructure and electrochemical performance of TCC-coated electrogalvanized steels. The TCC coating formed in a sulfate bath revealed a thin, compact, single-layer structure while two porous layers formed in a nitrate bath [41,42].

Figure 9 displays the simulated plots of the aqueous chemistry (a) in the mixture solutions of 0.024 M K_2ZrF_6 and 0.02 M $Cr(NO_3)_3$ and (b) in the mixture solutions of 0.024 M K_2ZrF_6 and 0.01 M $Cr_2(SO_4)_3$ at room temperature. The limiting pH values for zirconium oxide, chromium hydroxide and oxide deposits in both mixture solutions were the same at 2.1, 4.3 and 4.9, respectively. In addition, the fluoride concentrations increased with pH values in the range of pH 4 to pH 6. In such mixture solutions, fluoride ions were

the dominating anions leading to the same deposition limits for chromium and zirconium oxides and hydroxides.

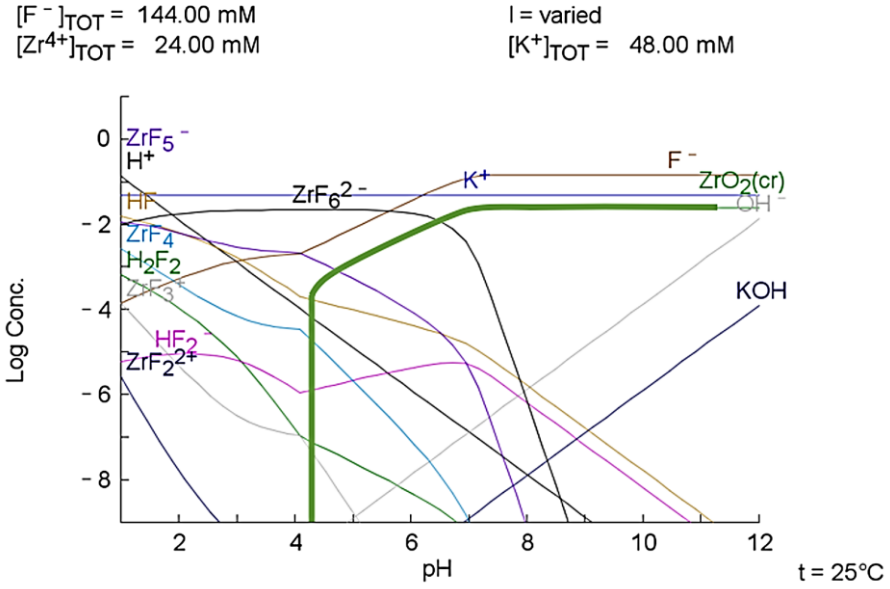


Figure 6. Simulated plots of the aqueous chemistry in the 0.024 M K_2ZrF_6 solution at room temperature.

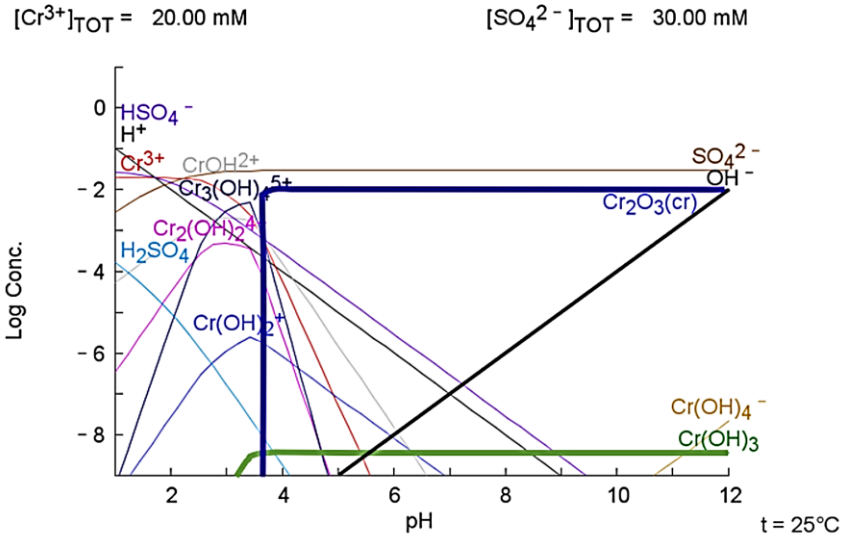


Figure 7. Simulated plots of the aqueous chemistry in 0.01 M $Cr_2(SO_4)_3$ solution at room temperature.

3.4. pH Evolution during Coating Formation and Raman Spectra of SurTec and Cr/Zr Solution

With consideration of the hydrolysis process of a weak acid nature of zirconium and chromium salts, the present work studied the pH evolution of bulk solutions of the mixture solutions of 0.02 M K_2ZrF_6 and 0.02 M $KCr(SO_4)_2$. Figure 10 displays the raw data and fitted line of pH values with dependence of the volume of 5 % NaOH droplets added into the mixture solutions of 0.02 M K_2ZrF_6 and 0.02 M $KCr(SO_4)_2$. The fitted line was functioned as "pH = –1.56 × exp(–volume/29.7) + 4.49" and indicated that the limiting pH values for the mixed solutions were 4.49. This is consistent with the previous simulation of the aqueous chemistry and the in-situ investigation of pH evolution during coating formation on aluminum and its alloys and magnesium alloys.

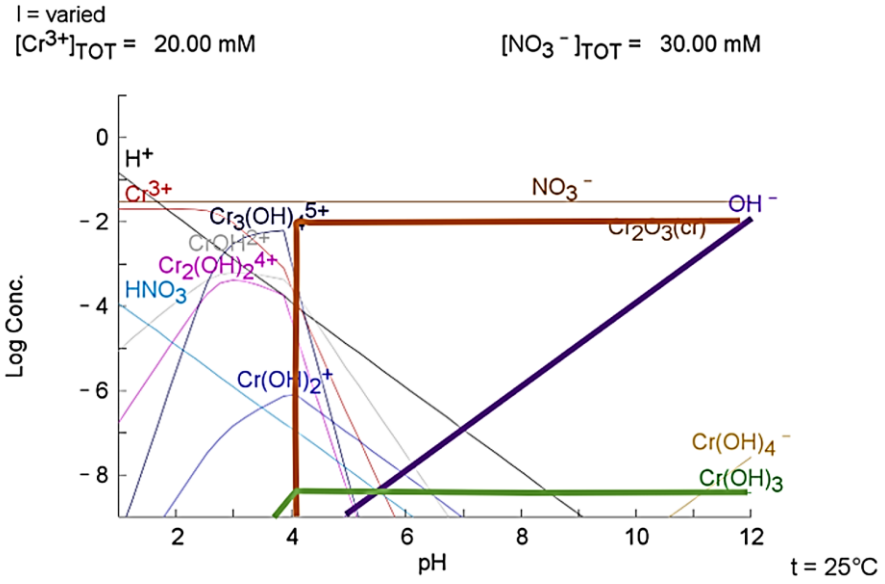


Figure 8. Simulated plots of the aqueous chemistry in 0.02 M $Cr(NO_3)_3$ solution at room temperature.

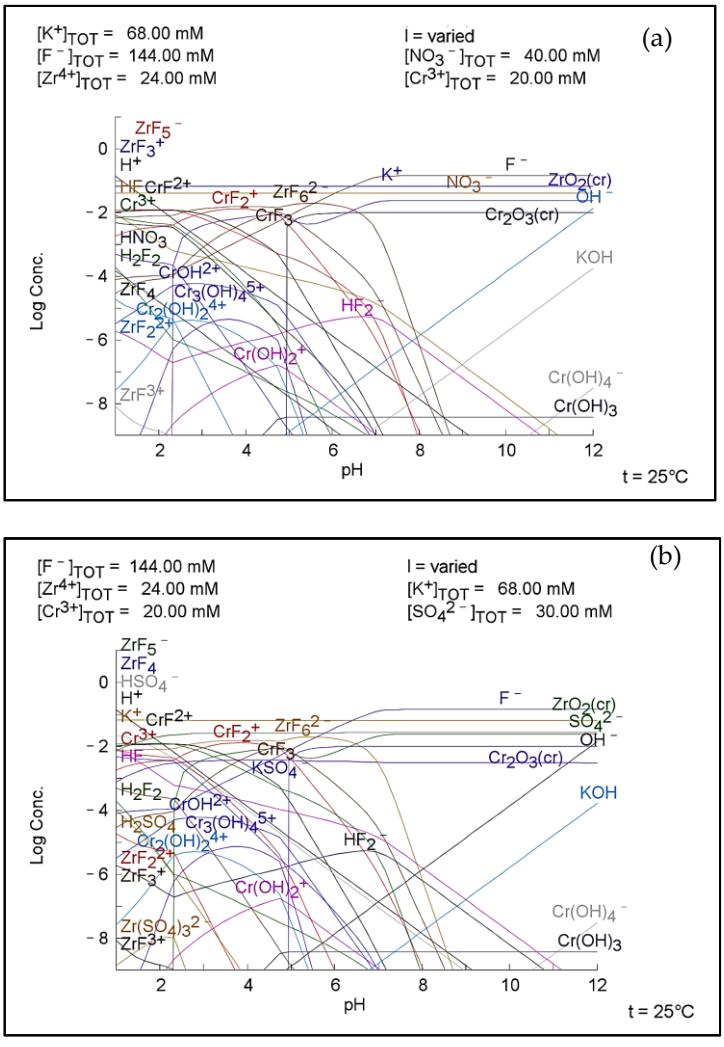


Figure 9. Simulated plots of species concentration relative to pH including (**a**) in the mixture solutions of 0.024 M K_2ZrF_6 and 0.02 M $Cr(NO_3)_3$ and (**b**) in the mixture solutions of 0.024 M K_2ZrF_6 and 0.01 M $Cr_2(SO_4)_3$ at room temperature.

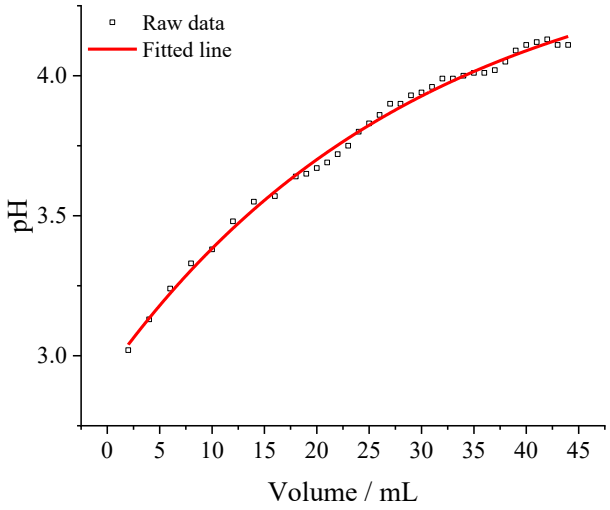


Figure 10. Plot of raw data and fitted line of pH values with dependence of the volume of 5 % NaOH droplets added into the mixture solutions of 0.02 M K_2ZrF_6 and 0.02 M $Cr(NO_3)_3$ and the fitted line was functioned as "pH = −1.56 × exp(−volume/29.7) + 4.49".

Figure 11 displayed Raman spectra of SurTec and Cr/Zr solution deposits when the bulk solution pH value was more than pH 7. The presence of chromium-, zirconium- and sulphate-containing salts was evidenced at the vibrational shifts at 536, 470 and 1060 (990) cm^{-1}, respectively. In this sense, the pH-driven solution deposits from the SurTec 650 ChromitAL and in-house Cr/Zr solutions had comparable chemistry.

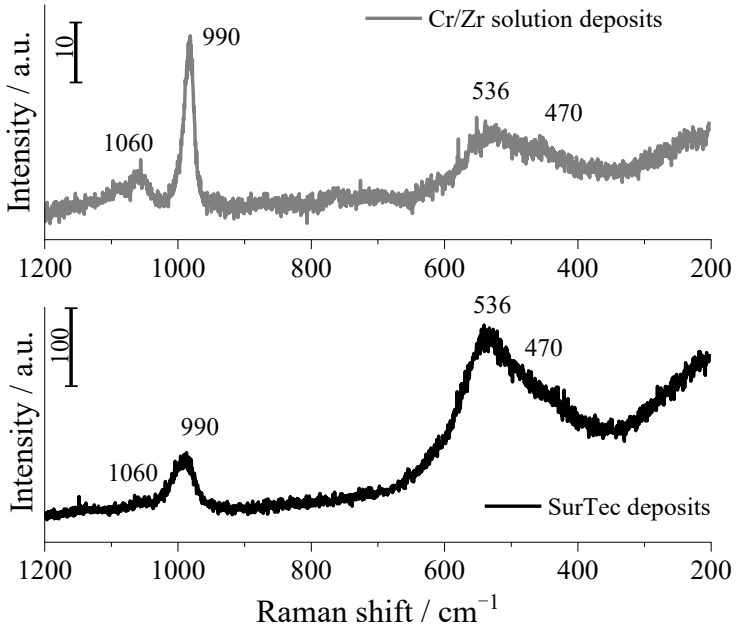


Figure 11. Raman spectrum of the solution deposits from the SurTec 650 ChromitAL and in-house Cr/Zr solution deposits when the pH value of the bulk solution was more than pH 7.

4. Conclusions

The present work employed a tungsten pH microelectrode to comparatively study the formation of trivalent chromium conversion (TCC) coatings on Al, AA 2024-T3 aluminum alloy and AZ91D magnesium alloys in SurTec ChromitAL solutions.

1. In sulfuric acid and TCC coating solutions, the open circuit potential of the microelectrode changes linearly with the pH value of the solution. The tungsten microelectrode

had a sensitivity of –60 mV/pH. The characteristics of the tungsten microelectrode was used to characterize the pH evolution of the metal–solution interface.
2. During the forming process of TCC coatings, the pH of the metal–solution interface changes. The peak and final pH values for pre-treated Al, AA 2024 alloy and AZ91D alloy were 4.9 and 3.5, 4.3 and 4.1, 4.7 and 3.5, respectively.
3. The interfacial pH evolution is associated with a hydrolysis process of the weak acid nature of zirconium and chromium salts, being the main components of TCC-coating solutions.
4. Raman spectra revealed the presence of chromium and zirconium oxides and sulphate in the solution deposits from Cr/Zr and SurTec solutions.

Author Contributions: Conceptualization, J.Q.; Data curation, W.S. and Z.Y.; Methodology. J.Q. and T.L.; Validation, N.W.; Writing—original draft W.S. and J.Q.: Writing—review & editing, G.B., L.J., J.P., J.Q. and T.L. All authors have read and agreed to the published version of the manuscript.

Funding: This work is supported by the National Natural Science Foundation of China (51701239), University–Industry Collaborative Education Program of MOE in China (BINTECH-KJZX-20220831-35), the Basic-Scientific-Research-Business-Fee Supporting Project of Henan Province (Grant No. 2021KY14) and Graduate Innovation Project from China University of Petroleum (East China) (YCX2020093).

Institutional Review Board Statement: Not applicable.

Informed Consent Statement: Not applicable.

Data Availability Statement: Not applicable.

Conflicts of Interest: The author declares no conflict of interest.

References

1. Hughes, A.E.; Taylor, R.J.; Hinton, B.R.W. Chromate Conversion Coatings on 2024 Al Alloy. *Surf. Interface Anal.* **1997**, *25*, 223–234. [CrossRef]
2. Bouali, A.; Serdechnova, M.; Blawert, C.; Tedim, J.; Ferreira, M.; Zheludkevich, M. Layered double hydroxides (LDHs) as functional materials for the corrosion protection of aluminum alloys: A review. *Appl. Mater. Today* **2020**, *21*, 100857. [CrossRef]
3. Zhou, P.; Yang, L.; Hou, Y.; Duan, G.; Yu, B.; Li, X.; Zhai, Y.; Zhang, B.; Zhang, T.; Wang, F. Grain refinement promotes the formation of phosphate conversion coating on Mg alloy AZ91D with high corrosion resistance and low electrical contact resistance. *Corros. Commun.* **2021**, *1*, 47–57. [CrossRef]
4. Wang, B.; Liu, X.; Wang, Y.; Ding, J.; Wei, S.; Xia, X.; Liu, M.; Xu, B. Microstructure and anti-corrosion properties of supersonic plasma sprayed Al-coating with Nano-Ti polymer sealing on AZ91-Magnesium alloy. *J. Mater. Res. Technol.* **2022**, *21*, 2730–2742. [CrossRef]
5. Dai, X.; Wu, L.; Xia, Y.; Chen, Y.; Zhang, Y.; Jiang, B.; Xie, Z.; Ci, W.; Zhang, G.; Pan, F. Intercalation of Y in Mg-Al layered double hydroxide films on anodized AZ31 and Mg-Y alloys to influence corrosion protective performance. *Appl. Surf. Sci.* **2021**, *551*, 149432. [CrossRef]
6. Egorkin, V.S.; Medvedev, I.M.; Sinebryukhov, S.L.; Vyaliy, I.E.; Gnedenkov, A.S.; Nadaraia, K.V.; Izotov, N.; Mashtalyar, D.V.; Gnedenkov, S.V. Atmospheric and Marine Corrosion of PEO and Composite Coatings Obtained on Al-Cu-Mg Aluminum Alloy. *Materials* **2020**, *13*, 2739. [CrossRef]
7. Rahmati, M.; Raeissi, K.; Toroghinejad, M.R.; Hakimizad, A.; Santamaria, M. Effect of Pulse Current Mode on Microstructure, Composition and Corrosion Performance of the Coatings Produced by Plasma Electrolytic Oxidation on AZ31 Mg Alloy. *Coatings* **2019**, *9*, 688. [CrossRef]
8. Egorkin, V.S.; Mashtalyar, D.V.; Gnedenkov, A.S.; Filonina, V.S.; Vyaliy, I.E.; Nadaraia, K.V.; Imshinetskiy, I.M.; Belov, E.A.; Izotov, N.V.; Sinebryukhov, S.L.; et al. Icephobic Performance of Combined Fluorine-Containing Composite Layers on Al-Mg-Mn–Si Alloy Surface. *Polymers* **2021**, *13*, 3827. [CrossRef]
9. Kendig, M.W.; Buchheit, R.G. Corrosion Inhibition of Aluminum and Aluminum Alloys by Soluble Chromates, Chromate Coatings, and Chromate-Free Coatings. *Corrosion* **2003**, *59*, 379–400. [CrossRef]
10. Gharbi, O.; Thomas, S.; Smith, C.; Birbilis, N. Chromate replacement: What does the future hold? *npj Mater. Degrad.* **2018**, *2*, 12. [CrossRef]
11. Mohammadi, I.; Shahrabi, T.; Mahdavian, M.; Izadi, M. Chemical modification of LDH conversion coating with diethyldithiocarbamate as a novel anti-corrosive film for AA2024-T3. *J. Ind. Eng. Chem.* **2021**, *95*, 134–147. [CrossRef]
12. Peltier, F.; Thierry, D. Review of Cr-Free Coatings for the Corrosion Protection of Aluminum Aerospace Alloys. *Coatings* **2022**, *12*, 518. [CrossRef]

13. Wei, H.; Tang, J.; Chen, X.; Tang, Y.; Zhao, X.; Zuo, Y. Influence of organic and inorganic cerium salts on the protective performance of epoxy coating. *Prog. Org. Coat.* **2022**, *166*, 106763. [CrossRef]
14. Pearlstein, F.; Agarwala, V.S. Trivalent Chromium Solutions for Applying Chemical Conversion Coatings to Aluminium Alloys or for Sealing Anodied Aluminium. *Plat. Surf. Finish* **1994**, *81*, 50–55.
15. Mitton, D.B.; Carangelo, A.; Acquesta, A.; Monetta, T.; Curioni, M.; Bellucci, F. Selected Cr(VI) replacement options for aluminum alloys: A literature survey. *Corros. Rev.* **2017**, *35*, 365–381. [CrossRef]
16. Qi, J.T.; Hashimoto, T.; Walton, J.; Zhou, X.; Skeldon, P.; Thompson, G. Trivalent chromium conversion coating formation on aluminium. *Surf. Coat. Technol.* **2015**, *280*, 317–329. [CrossRef]
17. Qi, J.; Thompson, G.E. Comparative studies of thin film growth on aluminium by AFM, TEM and GDOES characterization. *Appl. Surf. Sci.* **2016**, *377*, 109–120. [CrossRef]
18. Morose, G.; Pinsky, D.; Humphrey, C.; DeFranco, K. Evaluation of Conversion Coatings Without Hexavalent Chromium for Aerospace and Defense Applications. *J. Aerosp. Technol. Manag.* **2022**, *14*, e0522. [CrossRef]
19. Shahini, M.H.; Mohammadloo, H.E.; Ramezanzadeh, B. Recent advances in steel surface treatment via novel/green conversion coatings for anti-corrosion applications: A review study. *J. Coatings Technol. Res.* **2022**, *19*, 159–199. [CrossRef]
20. Samaei, A.; Chaudhuri, S. Role of zirconium conversion coating in corrosion performance of aluminum alloys: An integrated first-principles and multiphysics modeling approach. *Electrochim. Acta* **2022**, *433*, 14. [CrossRef]
21. Guo, Y.; Frankel, G. Characterization of trivalent chromium process coating on AA2024-T3. *Surf. Coatings Technol.* **2012**, *206*, 3895–3902. [CrossRef]
22. Qi, J.; Hashimoto, T.; Walton, J.; Zhou, X.; Skeldon, P.; Thompson, G.E. Formation of a Trivalent Chromium Conversion Coating on AA2024-T351 Alloy. *J. Electrochem. Soc.* **2016**, *163*, C25–C35. [CrossRef]
23. Li, L. Corrosion Protection Provided by Trivalent Chromium Process Conversion Coatings on Aluminium Alloys. Ph.D. Thesis, Michigan State University, East Lansing, MI, USA, 2013.
24. Qi, J.; Gao, L.; Li, Y.; Wang, Z.; Thompson, G.E.; Skeldon, P. An Optimized Trivalent Chromium Conversion Coating Process for AA2024-T351 Alloy. *J. Electrochem. Soc.* **2017**, *164*, C390–C395. [CrossRef]
25. Lee, Y.; Chu, Y.; Chen, F.; Lin, C. Mechanism of the formation of stannate and cerium conversion coatings on AZ91D magnesium alloys. *Appl. Surf. Sci.* **2013**, *276*, 578–585. [CrossRef]
26. Munson, C.A.; Swain, G.M. Structure and chemical composition of different variants of a commercial trivalent chromium process (TCP) coating on aluminum alloy 7075-T6. *Surf. Coat. Technol.* **2017**, *315*, 150–162. [CrossRef]
27. Stoica, A.-I.; Światowska, J.; Romaine, A.; Di Franco, F.; Qi, J.; Mercier, D.; Seyeux, A.; Zanna, S.; Marcus, P. Influence of post-treatment time of trivalent chromium protection coating on aluminium alloy 2024-T3 on improved corrosion resistance. *Surf. Coat. Technol.* **2019**, *369*, 186–197. [CrossRef]
28. Shruthi, T.K.; Walton, J.; McFall-Boegeman, S.; Westre, S.; Swain, G.M. Investigation of the Trivalent Chromium Process Conversion Coating as a Sealant for Anodized AA2024-T3. *J. Electrochem. Soc.* **2020**, *167*, 111504. [CrossRef]
29. Zhang, X.; Zhou, X.; Hashimoto, T.; Liu, B. Localized corrosion in AA2024-T351 aluminium alloy: Transition from intergranular corrosion to crystallographic pitting. *Mater. Charact.* **2017**, *130*, 230–236. [CrossRef]
30. Park, J.O.; Paik, C.; Alkire, R.C. Scanning Microsensors for Measurement of Local pH Distributions at the Microscale. *J. Electrochem. Soc.* **1996**, *143*, L174–L176. [CrossRef]
31. Li, L.; Desouza, A.L.; Swain, G.M. In situ pH measurement during the formation of conversion coatings on an aluminum alloy (AA2024). *Analyst* **2013**, *138*, 4398–4402. [CrossRef]
32. Saillard, R.; Zanna, S.; Seyeux, A.; Fori, B.; Światowska, J.; Blanc, C.; Marcus, P. Influence of ageing on the corrosion behaviour of 2024 aluminium alloy coated with a trivalent chromium conversion layer. *Corros. Sci.* **2021**, *182*, 109192. [CrossRef]
33. Ju, B.-F.; Chen, Y.-L.; Ge, Y. The art of electrochemical etching for preparing tungsten probes with controllable tip profile and characteristic parameters. *Rev. Sci. Instrum.* **2011**, *82*, 013707. [CrossRef] [PubMed]
34. Rahman, Z.; Das, A.K.; Chattopadhyaya, S. Fabrication of high aspect-ratio tungsten microtools through controlled electrochemical etching. *Mater. Manuf. Process.* **2021**, *36*, 1236–1247. [CrossRef]
35. Zhang, C.; Liao, S.; Yu, B.; Lu, X.; Chen, X.-B.; Zhang, T.; Wang, F. Ratio of total acidity to pH value of coating bath: A new strategy towards phosphate conversion coatings with optimized corrosion resistance for magnesium alloys. *Corros. Sci.* **2019**, *150*, 279–295. [CrossRef]
36. Chen, X.B.; Birbilis, N.; Abbott, T.B. Review of Corrosion-Resistant Conversion Coatings for Magnesium and Its Alloys. *Corrosion* **2011**, *67*, 035005-1. [CrossRef]
37. Dong, X.; Wang, P.; Argekar, S.; Schaefer, D.W. Structure and Composition of Trivalent Chromium Process (TCP) Films on Al Alloy. *Langmuir* **2010**, *26*, 10833–10841. [CrossRef]
38. Qi, J.; Gao, L.; Liu, Y.; Liu, B.; Hashimoto, T.; Wang, Z.; Thompson, G.E. Chromate Formed in a Trivalent Chromium Conversion Coating on Aluminum. *J. Electrochem. Soc.* **2017**, *164*, C442–C449. [CrossRef]
39. Verdalet-Guardiola, X.; Fori, B.; Bonino, J.-P.; Duluard, S.; Blanc, C. Nucleation and growth mechanisms of trivalent chromium conversion coatings on 2024-T3 aluminium alloy. *Corros. Sci.* **2019**, *155*, 109–120. [CrossRef]
40. Ning, G. Formation and Corrosion Resistance of Trivalent Chromium Conversion Coating on AZ91D Magnesium Alloys. Master's Thesis, China University of Petroleum (East China), Qingdao, China, 2020. Available online: https://kns.cnki.net/KCMS/detail/detail.aspx?dbname=CMFDTEMP&filename=1022634764.nh (accessed on 1 November 2022).

41. Wen, N.-T.; Lin, C.-S.; Bai, C.-Y.; Ger, M.-D. Structures and characteristics of Cr(III)-based conversion coatings on electrogalvanized steels. *Surf. Coat. Technol.* **2008**, *203*, 317–323. [CrossRef]
42. Wen, N.T.; Chen, F.J.; Ger, M.D.; Pan, Y.N.; Lin, C.S. Microstructure of Trivalent Chromium Conversion Coating on Electrogalvanized Steel Plate. *Electrochem. Solid-State Lett.* **2008**, *11*, C47–C50. [CrossRef]

Disclaimer/Publisher's Note: The statements, opinions and data contained in all publications are solely those of the individual author(s) and contributor(s) and not of MDPI and/or the editor(s). MDPI and/or the editor(s) disclaim responsibility for any injury to people or property resulting from any ideas, methods, instructions or products referred to in the content.